공학석사학위논문

Prediction on Pogo Phenomenon of a Space Launch Vehicle using the Virtual Mass and Modified Finite Element Method

가상질량기법과 개선된 유한요소법을 이용한 우주 발사체의 포고 현상 예측

2018 년 2 월

서울대학교 대학원

기계항공공학부

이 상 구

Prediction on Pogo Phenomenon of a Space Launch Vehicle using the Virtual Mass and Modified Finite Element Method

가상질량기법과 개선된 유한요소법을 이용한 우주 발사체의 포고 현상 예측

지도교수 신 상 준

이 논문을 공학석사 학위논문으로 제출함

2018 년 2 월

서울대학교 대학원

기계항공공학부

이 상 구

이상구의 공학석사 학위논문을 인준함

2018 년 2 월

위 원 장 _____ (인)

부위원장 _____ (인)

위 원 _____ (인)

Abstract

Prediction on Pogo Phenomenon of a Space Launch Vehicle using the Virtual Mass and Modified Finite Element Method

SangGu Lee

Department of Mechanical and Aerospace Engineering

The Graduate School

Seoul National University

In space launch vehicle, there exist many instabilities that can arise from the coupling between the structural and the feedline system. Therefore, it is required seriously to predict various instabilities in the development stage of the space launch vehicle. Pogo phenomenon is one of the coupling problems. Its phenomenon is an instability that the longitudinal modes of the launch vehicle structure resonate with the pressure and flow modes of the feedline in the propulsion system. And such resonance will re-excite the fuselage structure. For the analysis of the pogo phenomenon, accurate analysis of structural modes reflecting liquid propellant and feedline pressure mode in propulsion system will be needed. The purpose of this thesis is to conduct structural analysis of a three-dimensional tank with fluid and to predict the feedline pressure modes in a launch

vehicle. In addition, by applying a pogo suppressor in a feedline system, its prevention is implemented. The present pogo analysis is attempted on NASA space shuttle LOX system.

Three-dimensional tank structural modal analysis will be conducted using the virtual mass method. To verify the accuracy of this method, a 1/8-scale space shuttle external tank is estimated. Especially, the LOX tank in the external tank is analyzed intensively. The natural frequencies and mode shapes are found to be in good agreement with the existing document results.

In the feedline system, the present analysis will be adopted to predict the interpump line pressure modes causing instability of the space shuttle. Modified finite element method is verified by NASTRAN analysis and applied to the interpump line of the space shuttle LOX system. The comparison of numerical results against the reference about space shuttle are found to be satisfactory.

In addition, the pogo suppressor will be considered to the interpump line in the space shuttle. As a result, resonance area with the fuselage structure is prevented by varying the natural frequencies of the interpump line. In this way, the possibility of pogo suppression is confirmed.

Keywords : Space launch vehicle, Pogo phenomenon, Longitudinal modal analysis, Virtual mass method, Feedline pressure modes, Modified finite element method, Pogo suppressor

***Student Number* : 2016-20747**

Table of Contents

List of Figures

List of Tables

List of Symbols

Symbols	Meaning
$\nabla \cdot \vec{U}$	Dilatational strain
L_f	Fluid inertance
C_f	Fluid compliance
M_s	Structural mass
K_s	Structural stiffness
P	Dynamic pressure
U	Structural displacement
P_f	Pressure of the free surface
P_s	Pressure of the structural interface
P_i	Pressure of the internal fluid
U_f	Displacement of the free surface
U_s	Displacement of the structural interface surface
K_{ss}	Structural stiffness matrix
K_{ff}, K_{fs}, K_{sf}	Stiffness matrix due to the fluctuation of the ullage pressure and gravitational potential
A_{sf}^T, A_{fs}^T	Generalized area coupling partition
I_i	Fluid element inertance in a pipe
C_i	Fluid element compliance in a pipe
R_{fi}	Fluid element resistance in a pipe
Q_i^0	Fluid mean(steady) flow rate in a pipe
$[A]$	Fluid inertance matrix

$[C]$	Fluid compliance matrix
$[D]$	Fluid damping matrix
D_i	Fluid element diameter of a circular pipe
A_i	Fluid element area of a pipe
L_i	Fluid element length
L_e	Equivalent length for minor losses
a	Fluid acoustic speed
ρ	Fluid density
f	Friction factor of the pipe flow
C_a	Resistive Accumulator Compliance
R_a	Resistive Accumulator Resistance
L_a	Resistive Accumulator Inertance

Chapter 1

Introduction

1.1 Background and Motivation

In space launch vehicle, there exist many instabilities that can arise from the coupling between the structural and the propulsion system. One of those instabilities are the coupling between the axial modes of the launch vehicle fuselage structure and propulsion system. This longitudinal instability is called 'pogo' because the motion of this phenomenon looks like the pogo stick. This thesis is focused on the pogo phenomenon of a launch vehicle. The pogo phenomenon is caused by the structural characteristics of the space launch vehicle due to the typically long slender shape and relatively small mass ratio of such a vehicle. The mass ratio is the ratio of the structural only weight among the total vehicle weight including the propellant. Due to the high volume of the propellant in the launch vehicle, natural frequencies of the space launch vehicle will increase with the consumption of the liquid propellant. In Fig. 1.1, when the longitudinal natural frequencies of the vehicle fuselage match those of the pressure natural frequencies in feedline system, the perturbation of pressure/flow will be induced by affecting the change of thrust. Then, such mechanism constitutes a closed-loop system. As a result, the response amplitude of the entire vehicle will increase. For

that reason, the pogo phenomenon presents a safety hazard to the launch vehicle by damaging electronic components and decreasing momentarily the engine thrust while limiting the capability of the astronauts.

Most of the pogo phenomena were disclosed during the development phase of the space launch vehicle. Thus, reliable prediction of the pogo stability became inevitable during the early phase of the development process. Research related to the pogo phenomenon has been carried out consistently since the 60s [1-8], and it is still being considered in the development stage [9-14]. NASA published the space vehicle design criteria especially related with the pogo phenomenon [3~8]. Oppenheim proposed the comprehensive formulations for pogo analyses [9]. The practical pogo accidents occurred when the first longitudinal mode of the launch vehicle fuselage coincided with the first and second modes of the feedline. For example, as the liquid propellant decreased in the Saturn-V rocket, resonance of the engine with the first longitudinal mode of the vehicle fuselage caused the first-stage of F-1 engine to generate thrust oscillation [10].

Therefore, it is important to predict the longitudinal vibration mode of the launch vehicle fuselage and to analyze the pogo phenomenon by considering its coupling with the pressure mode in feedline system. This prediction is corresponds to the blue box process in Fig. 1.1. Furthermore, to avoid the resonance of the structural/feedline system, it is necessary to apply the pogo suppressor which lowers the natural frequencies of the feedline system.

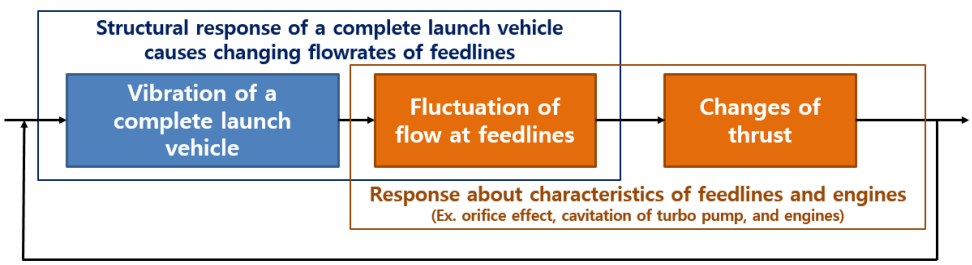

Figure 1.1 Closed Loop System of Pogo

1.2 Objectives and Thesis Overview

This thesis will be useful for pogo analysis by performing the following three steps; 1) longitudinal modal analysis of the LOX-filled tank, 2) pressure mode prediction of the inter-pump line, 3) pogo suppression analysis by applying a resistive accumulator.

The first step is the modal analysis of the three-dimensional tank filled with LOX as shown in Fig. 1.2. Because the tank occupies a large volume inside the space shuttle, it will influence upon the natural frequencies of the launch vehicle fuselage. The virtual mass method, one of the analytical methodologies on hydroelasticity, will be used to analyze the launch vehicle tank. This method will describe the propellant included in the tank as a relevant mass matrix. And then it will added to the mass matrix of the tank structure to finally perform the eigenvalue analysis. Especially, such method will be capable of predicting accurately the longitudinal mode of the tank.

The second step is prediction of the space shuttle inter-pump line pressure mode. According to Fig. 1.3 and Table 1.1, pogo instability in space shuttle LOX system will be caused when the interpump line modes coincide with the structural modes of space shuttle. This analysis is developed by changing the boundary conditions of the fluid end in the conventional finite element method as a function of element length and volume. Analysis on the pressure mode using the conventional finite element method was presented in Ref. 11. The modified finite element method discretizes the fluid into several elements, allowing continuous

analysis on the pressure modes of the entire fluid. In addition, by defining the boundary conditions with compliance C, which is a function of the volume, modified finite element method is capable of accurate prediction without considering the cross-sectional area of the interface. Therefore, it will become straightforward to analyze the pressure modes of the inter-pump line where the boundary condition is presented as compliance C.

The final step is the application of pogo suppressor by using the modified finite element method. By adding the pogo suppressor modeled by modified finite element method to the inter-pump line, the natural frequencies of the pressure mode are lowered below the pogo area. Consequently, the occurrence of the pogo phenomenon can be prevented.

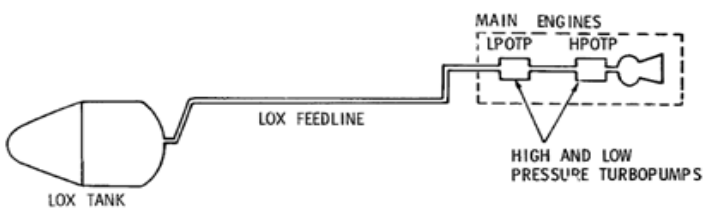

Figure 1.2 Scheme of the LOX Tank-Propulsion System [8]

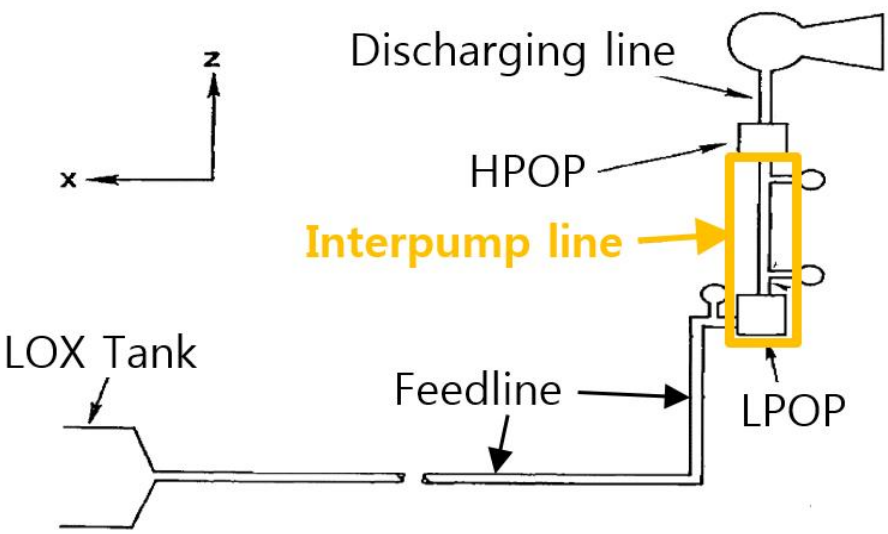

Figure 1.3 Pogo Model of the Space Shuttle LOX System

Table 1.1 Resonances of Structural/Interpump Line Mode in Space Shuttle

Structural mode	First feedline type mode	Interpump line mode
End-burn	Stable (at all structural mode)	E34-Destabilizing E35-Instability (24Hz)
After SRB Separation	A1-Instability (1.9~2.6Hz)	A46-Destabilizing (22~26Hz)
Lift-off	L1-Instability (2.2~2.6Hz)	L62-Destabilizing (23~24Hz)

Chapter 2

Analysis of the Longitudinal Modes

2.1 Formulation of Fluid-Structure Interaction

In a launch vehicle tank containing a fluid, a coupled analysis between the structure of the tank and the fluid inside the tank will be required because the fluid occupies a large volume of the overall component. Therefore, the analysis will be conducted after the proper formulation of the tank component is acquired while considering the fluid.

2.1.1 Hydroelastric Symmetric Formulation for a Tank with the Fluid

Certain equations are established as follows in order to analyze a tank containing a fluid, as shown in Fig. 2.1.

$$\dot{\vec{U}} = -\frac{1}{\rho}\nabla\hat{P} \tag{1}$$

$$\nabla\cdot\vec{U} = -\frac{1}{B}\dot{\hat{P}} \tag{2}$$

$$\hat{P} = \int_{-\infty}^{t} P\cdot dt \tag{3}$$

Equation (1) refers to the motion equation of the fluid particles, and Eq. (2) defines the constitutive relationship for a non-viscous, compressible fluid.

Additionally, Eq. (3) estimates the total pressure impulse. Based on Eqs. (1) - (3), the fluid in the tank can be described by the complementary Euler-Lagrange equation using Toupin's principle, as shown in Eq. (4). Also, as shown in Fig. 2.1, the equation for the tank structure can be formulated, as expressed by Eq. (5).

$$\left(L_f\right)P+\left(C_f\right)\ddot{P}=-\left(A^T\right)\ddot{U} \tag{4}$$

$$\left(M_s\right)\ddot{U}+\left(K_s\right)U=\left(A\right)P \tag{5}$$

Equation (4) and (5) are converted to Eq. (9) by applying Eqs. (6), (7), and (8). Equation (6) refers to the internal structural generalized force, and Eq. (7) defines the structural compliance. Equation (8) is used to determine the structural inertance.

$$\{F_s\}=\left(K_s\right)\{U\} \tag{6}$$

$$\left(C_s\right)=\left(K_s^{-1}\right) \tag{7}$$

$$\left(L_s\right)=\left(M_s^{-1}\right) \tag{8}$$

$$\begin{pmatrix} C_f & 0 \\ 0 & C_s \end{pmatrix}\begin{Bmatrix} \ddot{P} \\ \ddot{F}_s \end{Bmatrix}+\begin{pmatrix} L_f+A^TL_sA & -A^TL_s \\ -L_sA & L_s \end{pmatrix}\begin{Bmatrix} P \\ F_s \end{Bmatrix}=\begin{Bmatrix} 0 \\ 0 \end{Bmatrix} \tag{9}$$

Assuming that the fluid is incompressible, C_f will become zero in the complementary Euler-Lagrange matrix equation. Therefore, if Eq. (4) is represented in a matrix form, it will become equal to Eq. (10),

$$\begin{pmatrix} L_{ff} & L_{fs} & L_{fi} \\ L_{sf} & L_{ss} & L_{si} \\ L_{if} & L_{is} & L_{ii} \end{pmatrix}\begin{Bmatrix} P_f \\ P_s \\ P_i \end{Bmatrix}=-\begin{pmatrix} A_{ff}^T & A_{sf}^T \\ A_{fs}^T & A_{ss}^T \\ 0 & 0 \end{pmatrix}\begin{Bmatrix} \ddot{U}_f \\ \ddot{U}_s \end{Bmatrix} \tag{10}$$

With regard to an incompressible fluid for the structural dynamic equation of

Eq. (5), it can be expressed in terms of matrices, as shown in Eq. (11).

$$\begin{pmatrix} 0 & 0 \\ 0 & M_s \end{pmatrix} \begin{Bmatrix} \ddot{U}_f \\ \ddot{U}_s \end{Bmatrix} + \begin{pmatrix} K_{ff} & K_{fs} \\ K_{sf} & K_{ss} \end{pmatrix} \begin{Bmatrix} U_f \\ U_s \end{Bmatrix} = \begin{pmatrix} A_{ff} & A_{fs} & 0 \\ A_{sf} & A_{ss} & 0 \end{pmatrix} \begin{Bmatrix} P_f \\ P_s \\ P_i \end{Bmatrix} \tag{11}$$

If the internal fluid pressure P_i term is removed from Eq. (10), it can be summarized in terms of the free surface and structure, as shown in Eq. (13). Also, P_i is expressed by Eq. (12).

$$\{P_i\} = -(L_{ii})^{-1} \begin{pmatrix} L_{if} & L_{is} \end{pmatrix} \begin{Bmatrix} P_f \\ P_s \end{Bmatrix} \tag{12}$$

$$\begin{gathered} \begin{pmatrix} L'_{ff} & L'_{fs} \\ L'_{sf} & L'_{ss} \end{pmatrix} \begin{Bmatrix} P_f \\ P_s \end{Bmatrix} = -\begin{pmatrix} A^T_{ff} & A^T_{sf} \\ A^T_{fs} & A^T_{ss} \end{pmatrix} \begin{Bmatrix} \ddot{U}_f \\ \ddot{U}_s \end{Bmatrix}, \\ \begin{pmatrix} L'_{ff} & L'_{fs} \\ L'_{sf} & L'_{ss} \end{pmatrix} = \begin{pmatrix} L_{ff} & L_{fs} \\ L_{sf} & L_{ss} \end{pmatrix} - \begin{pmatrix} L_{fi} \\ L_{si} \end{pmatrix} (L_{ii})^{-1} \begin{pmatrix} L_{if} L_{is} \end{pmatrix} \end{gathered} \tag{13}$$

However, a singularity will occur in the matrix of Eq. (13) because an incompressible fluid does not contract under uniform pressure. Therefore, the free surface pressure P_f can be set to be zero to solve such singularity. When P_f =0, the ullage and gravitational stiffness K_{ff}, K_{fs} and K_{sf} can be ignored. Thus, Eq. (13) can be re-expressed, as in Eqs. (14) and (15).

$$\left(L'_{fs}\right)\{P_s\} = -\left(A^T_{ff}\right)\{\ddot{U}_f\} - \left(A^T_{sf}\right)\{\ddot{U}_s\} \tag{14}$$

$$\left(L'_{ss}\right)\{P_s\} = -\left(A^T_{fs}\right)\{\ddot{U}_f\} - \left(A^T_{ss}\right)\{\ddot{U}_s\} \tag{15}$$

If the displacement of the free surface is perpendicular to the free surface, the generalized area coupling partition A^T_{sf}, A^T_{fs} will be equal to zero. In such a case, Eqs. (14) and (15) are converted to Eqs. (16) and (17) respectively.

$$\left(L_{fs}^{'}\right)\{P_s\} = -\left(A_{ff}^{T}\right)\{\ddot{U}_f\} \tag{16}$$

$$\left(L_{ss}^{'}\right)\{P_s\} = -\left(A_{ss}^{T}\right)\{\ddot{U}_s\} \tag{17}$$

Equation (18) is a summation of Eq. (17) in terms of P_s. In addition, substituting Eq. (18) into the structural dynamic equation of Eq. (5) yields Eq. (19).

$$\{P_s\} = -\left(L_{ss}^{'}\right)^{-1}\left(A_{ss}^{T}\right)\{\ddot{U}_s\} \tag{18}$$

$$\left(M_s + M_f\right)\{\ddot{U}_s\} + \left(K_{ss}\right)\{U_s\} = \{0\}, \quad \left(M_f\right) = \left(A_{ss}\right)\left(L_{ss}^{'}\right)^{-1}\left(A_{ss}^{T}\right) \tag{19}$$

Therefore, if the following assumptions are used, i.e., 1) the fluid in the tank is assumed to be incompressible, 2) the fluid is inviscid, 3) the pressure at the surface of the fluid in the tank P_f is zero, 4) the displacement of the fluid surface is perpendicular to the surface of the fluid, the fluid in the tank will be expressed only in terms of the fluid mass matrix. Therefore, the equation of motion for the tank containing the fluid can be established as shown in Eq. (19). $L_{ss}^{'}$ is the structural inertance matrix and K_{ss} becomes equal to K_s.

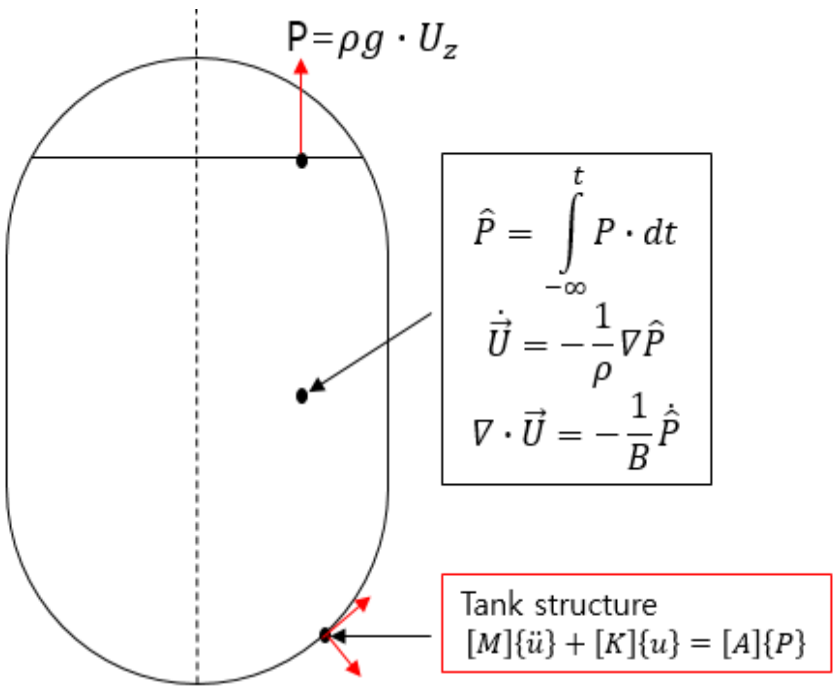

Figure 2.1 Scheme and Formulation of a Tank with Fluid

2.1.2 Virtual Mass Method

When a liquid propellant influences the dynamic response of a structure such as a launch vehicle tank, the virtual mass method, included in NASTRAN, can be used to analyze the hydroelastic effect of the launch vehicle tank and the fluid in the tank. By this method, the fluid in the tank is constructed in the form of a mass matrix using Helmholtz method. The Helmholtz method distributes a fluid source with a simple solution of differential equations over the element to which the fluid is applied. And the velocity vector $\dot{u}_i$ and pressure p_i for each element are derived through the interaction between the elements. $\dot{u}_i$ and p_i are expressed correspondingly by Eqs. (20) and (21).

$$\dot{u}_i = \sum_j \int_{A_j} \frac{\sigma_j e_{ij}}{\left| r_i - r_j \right|^2} dA_j \tag{20}$$

$$p_i = \sum_j \int_{A_j} \frac{\rho \dot{\sigma}_j e_{ij}}{\left| r_i - r_j \right|} dA_j \tag{21}$$

r_j is the element location at j, A_j is the element area at j, r_i is any other point i except j, and e_{ij} denotes the unit vector in the direction from j to i. Eq. (22) is obtained by summarizing the velocity vector with respect to the source. In Eqs. (21) and (23), the load acting on the element is obtained by integrating the pressure p_i against the area A_j.

$$\{\dot{u}\} = [\chi][\sigma] \tag{22}$$

$$\{F\} = [\Lambda][\dot{\sigma}] \tag{23}$$

Thus, by differentiating Eq. (22) with respect to time and with substitution into Eqs. (23) and (24), the mass matrix of the fluid can be obtained.

$$\{F\} = \left[M_f\right][\ddot{u}], \qquad \left[M_f\right] = [\Lambda][\chi]^{-1} \tag{24}$$

The assumptions used in the virtual mass method are as follows:

1. The fluid in the tank is incompressible and inviscid.
2. The fluid has a uniform density.
3. The fluid in the tank must define a free surface.
4. Pressure on the free surface is zero.
5. Fluid effects such as gravity, surface waves, and steady flows are ignored.

For a small hemispherical tank and the space shuttle 1/8-scale external tank , the surface of the fluid in the tank is located perpendicular to the axis of the tank. For its pogo analysis, the longitudinal modes in which the displacement of the fluid surface moves perpendicularly to the fluid surface are now obtained. Therefore, because the virtual mass method satisfies all the assumptions (Assumptions 1 through 4), hydroelastic analysis of the tank in its longitudinal direction will be conducted using the virtual mass method.

2.2 Modal Analysis for a Tank filled with Fluid

2.2.1 Verification of the Virtual Mass Method

To verify the hydroelastic analysis of a tank containing a fluid using the virtual mass method, the aluminum tank used in a longitudinal mode test at the Southwest Research Institute (SwRI) is selected as the object of analysis. The shape of the experimental hardware is shown in Fig. 2.2, and the relevant information and properties are summarized in Table 2.1.

In Fig. 2.3, the present object is discretized using a three-dimensional shell element and constrained in terms of its six degrees of freedom as the boundary condition of the edge. The elements used are QUAD4 and Tria3 elements. The total number of elements is 2240, and the number of nodes is 2241.

The longitudinal modal analysis is conducted with the height of the liquid in the tank (h) divided by the diameter of the tank (D) values ranging from 0 to 0.5 at 0.1 intervals. The modal analysis is performed up to the fourth order so as to compare the outcomes with the experimental results. In Fig. 2.4, the present numerical predictions are plotted as circles and the experimental results are plotted with the other shapes.

At the first to the fourth longitudinal natural frequencies, as shown in Fig. 2.4, it is found that the experimental results and the numerical predictions are well correlated. Especially when the value of the height of the liquid in the tank divided by the diameter of the tank is 0.5, as given in Table 2.2, the maximum discrepancy

is within 10%. The mode shapes for the first to fourth longitudinal modes in Fig. 2.5 are highly consistent with the experimental results. Thus, it is confirmed that the virtual mass method would be an appropriate method for longitudinal modal analyses of tanks containing fluids.

Table 2.2 Parameters of the Small Aluminum Hemispherical Bulkheads [1]

Structural Element	Equation of Surface	Inside Diameter (m)	Material Density $\left(kg/m^3\right)$	$E\times10^6$ (Pa)
Bulkhead	$x^2+y^2=5^2$	D=0.254	2712.65	68900

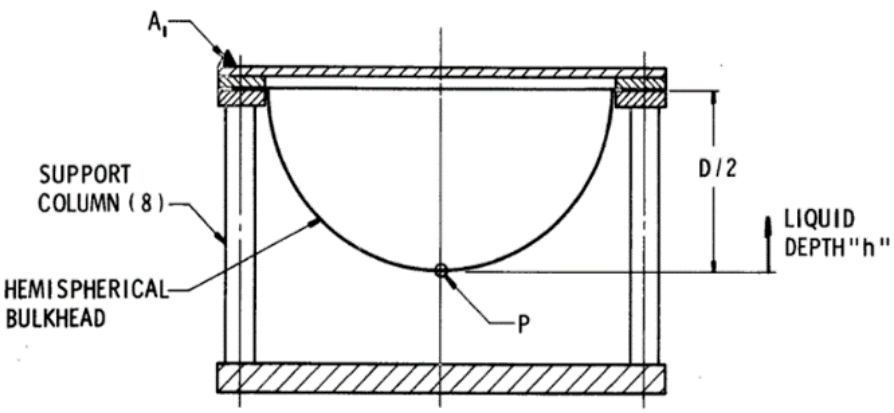

Figure 2.2 Configuration of the Small Aluminum Hemispherical Bulkheads [1]

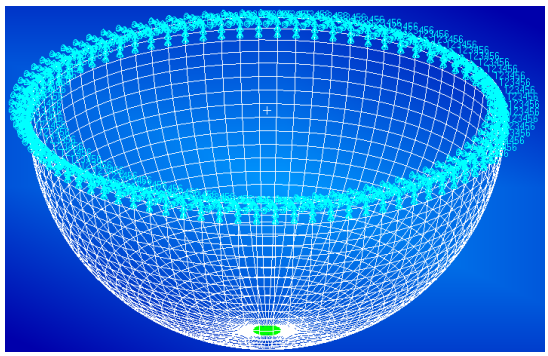

Figure 2.3 Small Hemispherical Tank NASTRAN Discretization

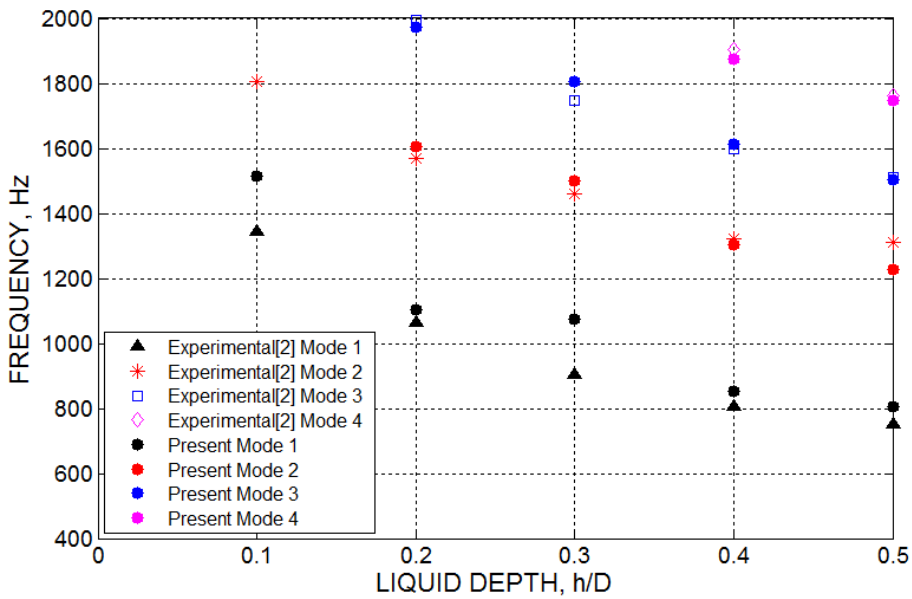

Figure 2.4 Comparison of the Natural Frequencies with respect to the height of the liquid in the tank divided by the diameter of the tank

Table 2.2 Comparison of Experimental/Analytically Predicted Natural Frequencies

(Height of the Liquid in the Tank divided by Diameter of the Tank=0.5)

Longitudinal mode	SwRI Measured Frequencies [Hz] (Experimental results)	Present method [Hz] (Analytical prediction)	Difference (%)
1st	750	804	7.19
2nd	1310	1226	6.43
3rd	1510	1504	0.40
4th	1760	1747	0.71

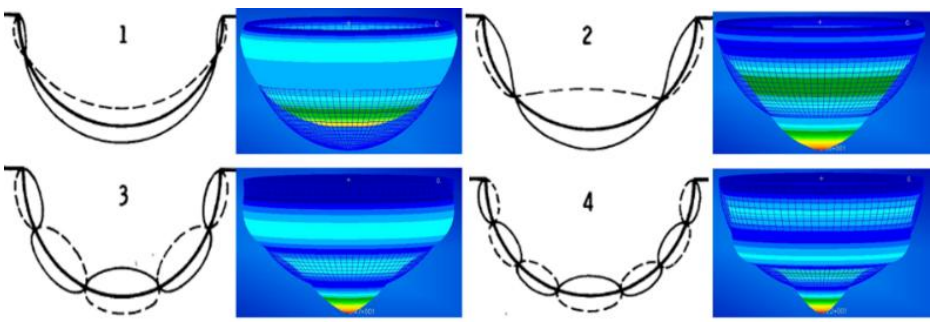

Figure 2.5 Mode Shapes of the Small Hemispherical Tank Longitudinal Mode

2.2.2 Application of the Virtual Mass Method

In the NASA space shuttle, there was an external tank containing a liquid oxygen tank with a liquid hydrogen tank to its side. Both liquid oxygen and hydrogen as propellants were supplied to the engine of the space shuttle via a feedline. There existed many thin and long pipes between the tank and the engine. Specifically, the feedline length between the LOX tank and the engine was quite long given the long distance between the two components. Moreover, because the density of liquid oxygen is greater than that of liquid hydrogen, the potential for the pogo phenomenon to arise in the LOX tank was high.

Therefore, the virtual mass method is utilized to analyze the external tank by focusing on the longitudinal mode of the LOX tank. Its 1/8-scale external tank with an earlier experimental modal observation and the NASTRAN modal prediction are selected to devise the object configuration [3]. As shown in Fig. 2.6, the objective of the present analysis consists of the following four components: a liquid-oxygen tank, an inter-tank skirt, a liquid-hydrogen tank, and an aft tank skirt. The height of the liquid in the tank would be prescribed in accordance with the categories of lift off, post max Q, and empty. The first longitudinal vibration modal analysis for the external tank and the LOX tank would then be conducted for each height category of the liquid.

The configuration, properties, and boundary conditions of the space shuttle 1/8-scale external tank are established by referring to the literature (Ref. 5). When the height of the liquid corresponds to the lift-off level, the numbers of elements

would be 4,448 for QUAD4, 128 for Tria3, and the total number of nodes is 4,484. In the case of the post-max Q level and the empty level, the numbers of elements are 4,288 for QUAD4, 128 for Tria3, with 4,324 nodes in total.

Figs. 2.7~2.11 show that the present numerical prediction is well correlated with those in the literature (Ref. 5). Specifically, the longitudinal modal shape of the LOX tank section would be the major result of the present analysis. For the post-max Q level, the LOX N=0 DOME mode, which is the first longitudinal mode of the LOX tank, and the second longitudinal mode of the external tank, are also analyzed.

Table 2.3 shows that there is a slight difference between the previous experiments, the existing numerical prediction found in the references (Ref. 5), and the present prediction obtained by the virtual mass method regarding the natural frequencies. The current discrepancies arise because the stiffness coefficients of the ring frame used to reinforce the outer tank shell is not taken into account and the external tank configuration is a slightly different from the actual hardware in terms of the thickness and structural shape. However, even with such differences, the correlations among the experimental results and numerical predictions in the literature (Ref. 5) and the present prediction outcomes obtained by the virtual mass method are found to be satisfactory.

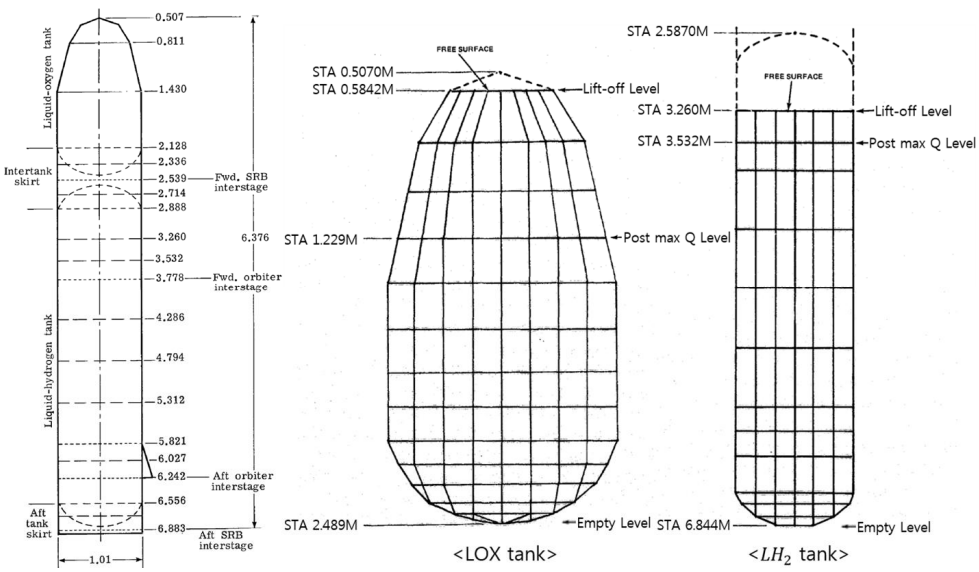

Figure 2.6 Schematic of the 1/8-scale Space Shuttle External Tank [5, 6]

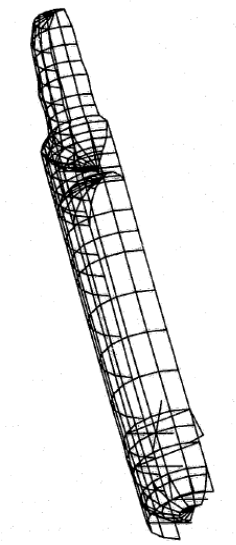

(a) Original discretization used in Ref. 5

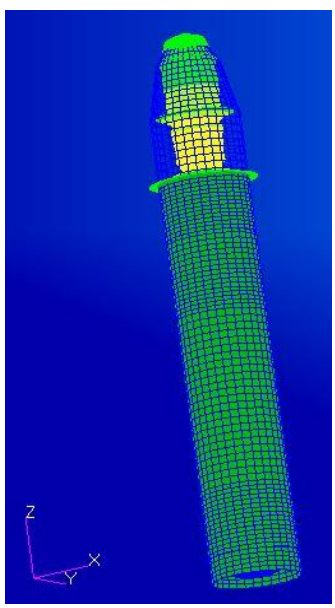

(b) Present discretization

Figure 2.7 First Longitudinal Mode Shape at the Lift-off Level

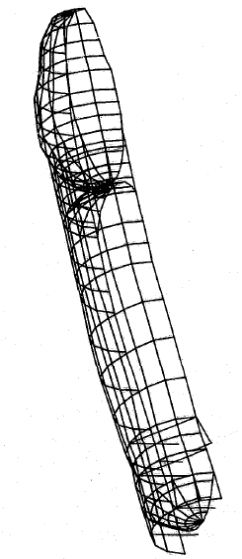

(a) Original discretization used in Ref. 5

(b) Present discretization

Figure 2.8 First Longitudinal Mode Shape at the Post-max Q Level

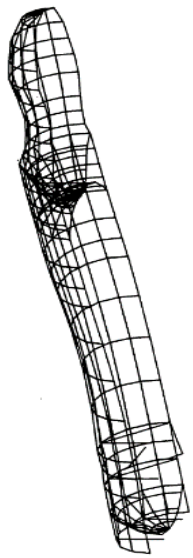

(a) Original discretization used in Ref. 5

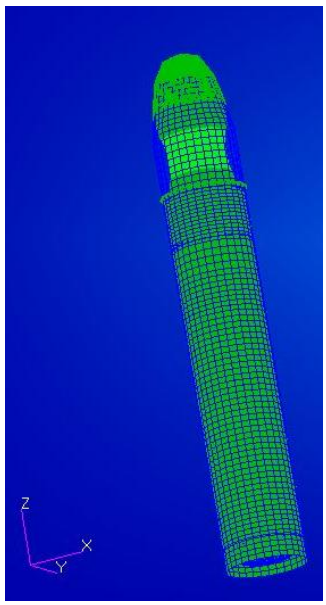

(b) Present discretization

Figure 2.9 Second Longitudinal Mode Shape at the Post-max Q Level

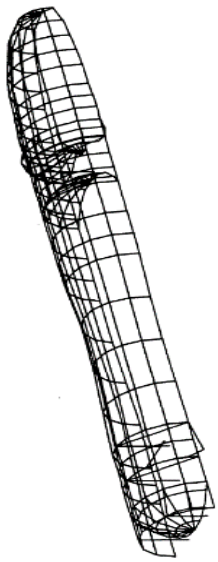

(a) Original discretization used in Ref. 5

(b) Present discretization

Figure 2.10 LOX N=0 DOME Mode Shape at the Post-max Q Level

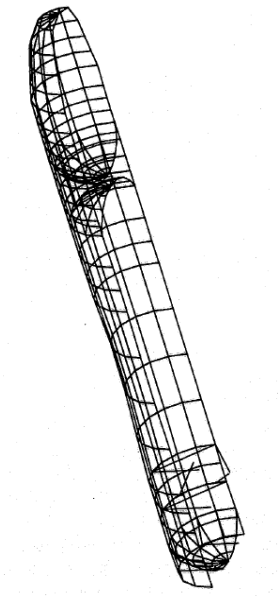

(a) Original discretization used in Ref. 5

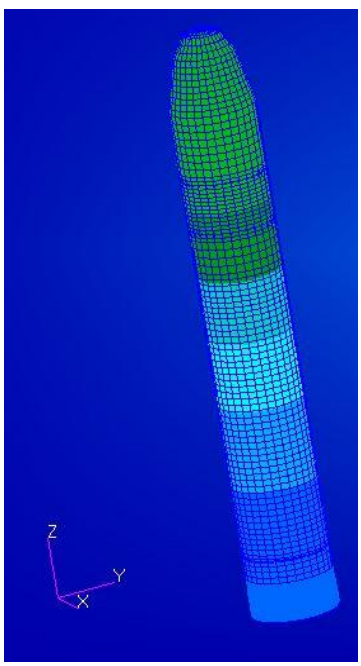

(b) Present discretization

Figure 2.11 First Longitudinal Mode Shape at the Empty Level

Table 2.3 Comparison with Ref. 5 regarding the Natural Frequencies

Longitudinal modes	Ref. 5 (Hz)	Present method (Hz)
First longitudinal(Lift off)	29.7 (NASA NASTRAN data)	20.3
First longitudinal(Post max Q)	49.0 (test data)	39.4
Second longitudinal(Post max Q)	79.2 (NASA NASTRAN data)	75.7
LOX N=0 DOME(Post max Q)	113.7 (NASA NASTRAN data)	109.9
First longitudinal(Empty)	257.8 (NASA NASTRAN data)	254.8

Chapter 3

Analysis of the Feedline System

3.1 Analysis of the Pipe Pressure Modes

In a fluid included inside a pipe, it is essential to do preliminary observations on the pressure modes and natural frequencies in order to predict the magnitude of pressure and flow vibration. It is especially required at the locations where those quantities cannot be acquired due to limitation of experiments. Such estimation provides valuable diagnostic information for dynamic characteristics at the propellant feedline of a space launch vehicle. In particular, it is useful to predict pressure modes analytically in the case of the pogo phenomenon in which the pressure perturbation of the feedline causes instability. Thus, a systematic fluid element approach was attempted in the past to analyze the pressure modes of fluid included inside a pipe.

For example, in Ref. 9, analysis on the pressure modes was performed by assuming that the fluid was filled in the one-dimensional straight pipe and divided the fluid into several elements. Therefore, the pressure P and the volume flow rate Q of the *i*-th element are predicted with the I_i, C_i, and R_{fi}, using the governing Eqs. (25) and (28), respectively.

$$I_i \dot{Q}_i = P_i - P_{i+1} - R_{fi} |Q_i| Q_i \tag{25}$$

$$I_i = \frac{\rho L_i}{A_i} \tag{26}$$

$$R_{fi} = \frac{\rho}{2A_i^2} f\left(\frac{L_i + L_e}{D_i}\right) \tag{27}$$

Equation (25) can be obtained by integrating an one-dimensional momentum equation and ignoring the convection effect of the fluid.

$$C_i \dot{P}_i = Q_{i-1} - Q_i \tag{28}$$

$$C_i = \frac{A_i L_i}{\rho a^2} \tag{29}$$

Equation (28) is the conservation of the mass, assuming an isentropic flow of an ideal gas.

$$[C]\ddot{P} + [H]\dot{P} + [E_P]P = 0 \tag{30}$$

$$[H] = B^T [A]^{-1} [D] \left[B^T\right]^{-1} [C] \tag{31}$$

$$[E_P] = B^T [A]^{-1} B \tag{32}$$

$$[C] = \begin{bmatrix} C_1 & & & \\ & C_2 & & \\ & & \ddots & \\ & & & C_N \end{bmatrix} \quad B = \begin{bmatrix} -1 & 1 & & \\ & -1 & 1 & \\ & & \ddots & 1 \\ & & & -1 \end{bmatrix}$$

$$[A] = \begin{bmatrix} I_1 & & & \\ & I_2 & & \\ & & \ddots & \\ & & & I_N \end{bmatrix} \quad [D] = \begin{bmatrix} 2R_{f1}Q_1^0 & & & \\ & 2R_{f2}Q_2^0 & & \\ & & \ddots & \\ & & & 2R_{fN}Q_N^0 \end{bmatrix} \tag{33}$$

When an one-dimensional straight pipe is divided into N elements, Eq. (30) can be obtained as the governing equations. Equation (30) is an ordinary differential equation relating pressures. By using Eq. (30), eigenvalue analysis of the fluid is performed and pressure modes can be predicted.

3.1.1 The Modified Finite Element Method

In the pressure modes of the fluid in the pipe, the natural frequencies and mode shapes can vary depending on the boundary conditions at both ends of the fluid. In other words, the value of inertance I_1, I_N and compliance C_1, C_N greatly affects the boundary conditions. In Equations (26) and (29), assuming that the fluid flowing in the pipe is the same, the cross-sectional area and the length of the element at both ends of the fluid will become variables of the boundary condition. However, when two pipes with different cross-sectional areas are connected, it is difficult to select the correct cross-sectional area at the pipe boundary.

In this case, the boundary condition between the pipes can be treated as the fluid volume of the boundary element. As shown in Fig. 3.1, the term of cross-sectional area is removed from the inertance and compliance formulas, and the length/volume of the element are used as variables. This is the modification on the existing finite element method formula and is quoted to as the modified finite element method. Therefore, more accurate boundary conditions will be applicable. Also, since the compliance C can be derived from the fluid flow experiment in the pipe, the fluid volume at the pipe boundary will be easily obtained. Thus, the modified finite element method is used to build the present analysis.

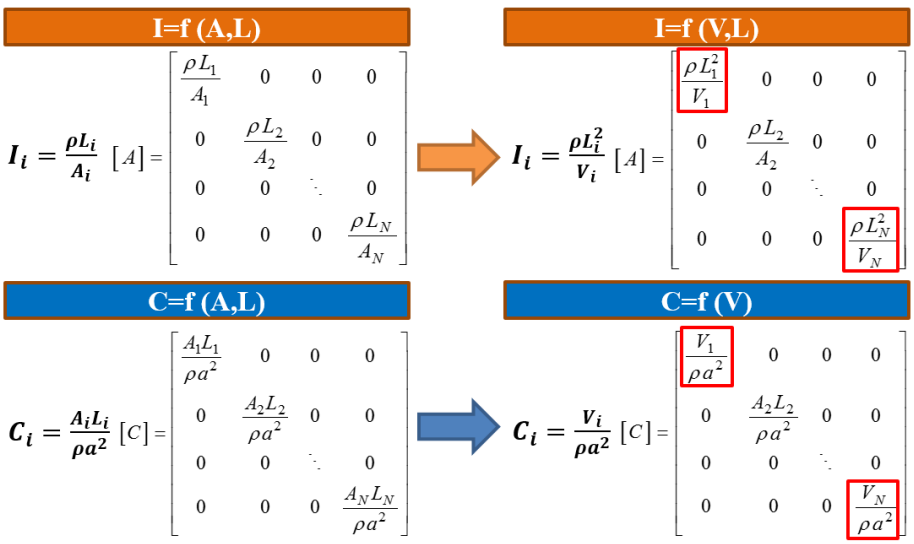

Figure 3.1 Definition of the Modified Finite Element Method

3.2 Verification and Application for Feedline System

3.2.1 Verification of the Modified Finite Element Method

As shown in Fig. 3.2, an object is selected as helium gas which has the same shape as the pipe. And, volumetric values at both ends of the fluid are divided into two cases to compare the natural frequencies. In Table 3.1, Case (A) is a closed-closed system and Case (B) is a closed-open system [11]. The natural frequencies of Case (A) and (B) are determined by the present analysis. Eigenvalue analysis in the present analysis is conducted by using the 'eig' function in MATLAB. And, the modified finite element method used in the present analysis only considers an undamped system, i.e., damping term $[D]$ is set to be zero.

To verify the present analysis, Case (A) and (B) are obtained up to the 10^{th} mode and compared with the NASTRAN results. In the present analysis, 200 elements and 201 degrees of freedom are used in both cases. And, the wave length is derived to obtain the NASTRAN result up to the 10^{th} mode. The wave length is the speed of sound divided by the 10^{th} natural frequency, which is the maximum natural frequency of the region of interest. Because at least 6 elements are required to characterize the wave length, the maximum element size is the wave length divided by 6.

In the Case (A), since the natural frequency range of the 10^{th} mode is approximately 1970~2010Hz, the maximum element size is 0.0835m or less. Therefore, the elements of the NASTRAN model are 4 in the radial direction of the

pipe section, 24 in the circumferential direction, and 100 in the pipe length direction. Because the closed-closed condition is not given a boundary condition, the number of degrees of freedom is 9797. The results of natural frequencies comparison with present analysis are shown in Table. 3.2, and the maximum discrepancy is -0.74%, which is a reasonable value. And, in Fig. 3.3~6 (a), the mode shape is also exactly the same.

In the Case (B), because the natural frequency range of the 10^{th} mode is 1870~1910Hz, the maximum element length is 0.0879m or less. Therefore, the meshing is the same as Case (A). In the boundary condition, the degree of freedom with respect to pressure corresponds to the X direction displacement of each node. Since the free surface of the open condition is zero pressure, the node of the open end of the fluid is UX=0. Therefore, the degree of freedom is 9700. Comparison of the natural frequencies with the present analysis is in good agreement with the maximum discrepancy of -0.28% as shown in Table 3.3. The results of natural frequencies. Also, the mode shapes are similar to present analysis as shown in Fig. 3.3~6 (b).

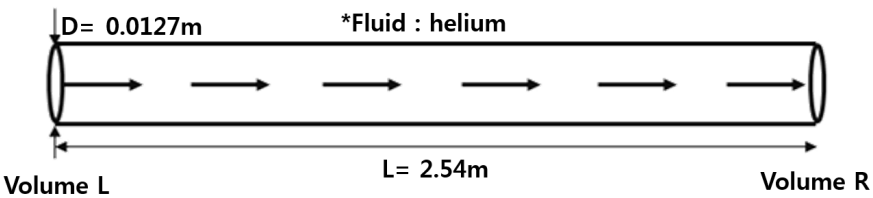

Figure 3.2 Object for Verification of the modified Finite Element Method

Table 3.1 Two Cases of Fluid End Volume Condition [11]

Case	Volume L (m^3)	Volume R (m^3)
A	1.64×10^{-10} (Closed system)	1.64×10^{-10} (Closed system)
B	1.64×10^{-10} (Closed system)	1.64×10^{-1} (Open system)

Table 3.2 Comparison of the Pressure Frequencies for Case (A)

Case A	Present analysis [Hz] [No. of DOF's=201]	NASTRAN [Hz] [No. of DOF's=9,797]	Difference (%)
1st mode	199.6	198.2	-0.74
2nd mode	398.6	396.4	-0.57
3rd mode	597.8	594.7	-0.51
4th mode	796.9	793.2	-0.47
5th mode	995.9	991.8	-0.42
6th mode	1195.0	1190.7	-0.36
7th mode	1393.9	1389.9	-0.29
8th mode	1592.8	1589.5	-0.21
9th mode	1791.6	1789.4	-0.12
10th mode	1990.2	1989.8	-0.02

Table 3.3 Comparison of the Pressure Frequencies for Case (B)

Case B	Present analysis [Hz] [No. of DOF's =201]	NASTRAN [Hz] [No. of DOF's =9,700]	Difference (%)
1st mode	99.4	99.1	-0.28
2nd mode	298.1	297.3	-0.27
3rd mode	496.8	495.5	-0.25
4th mode	695.4	693.9	-0.22
5th mode	894.1	892.5	-0.18
6th mode	1092.6	1091.2	-0.13
7th mode	1291.1	1290.3	-0.07
8th mode	1489.6	1489.6	0.00
9th mode	1687.9	1689.4	0.09
10th mode	1886.1	1889.5	0.18

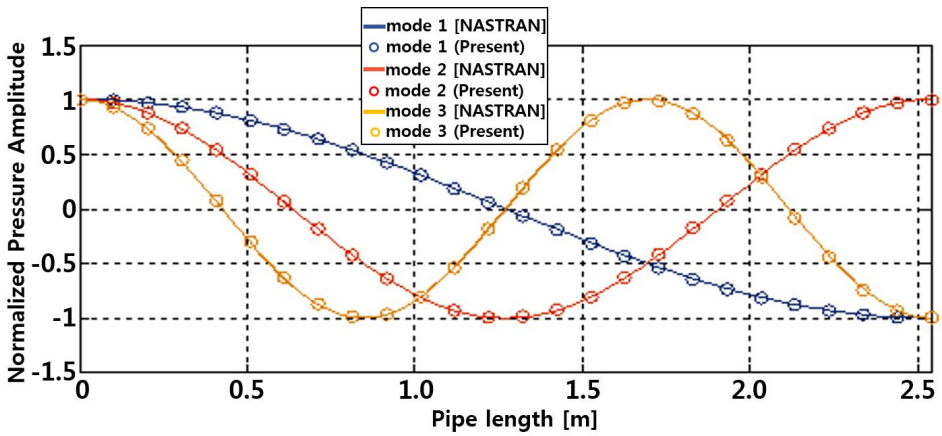

(a) Case (A)

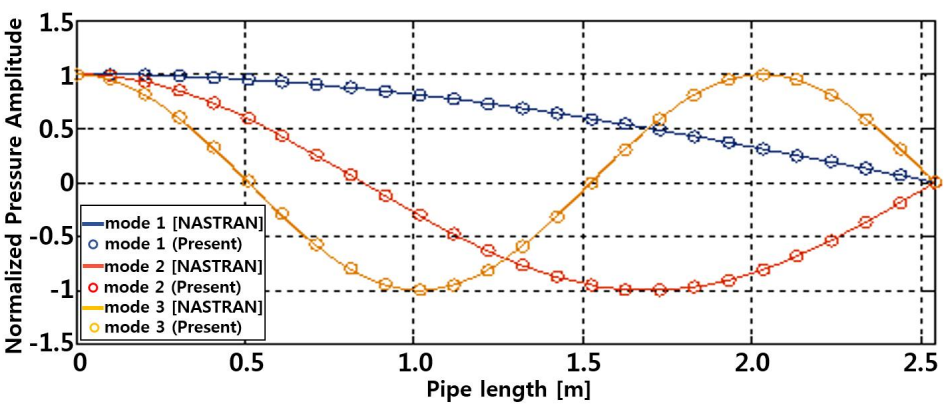

(b) Case (B)

Figure 3.3 Shapes for the 1st~3rd Pressure Modes

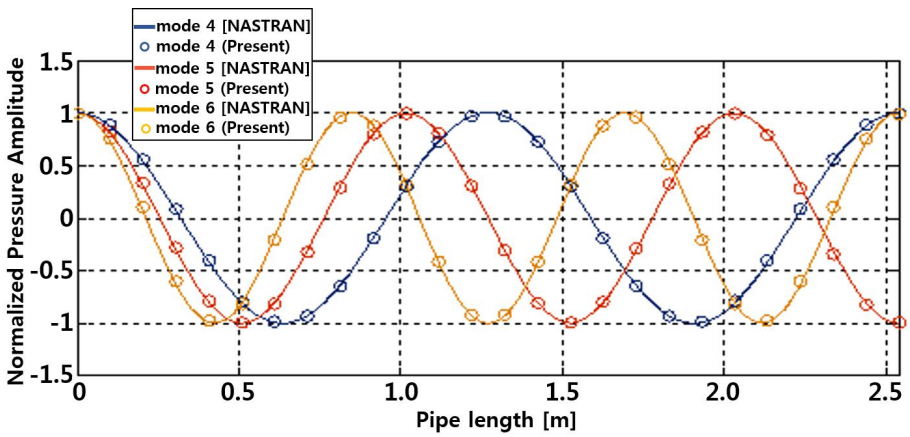

(a) Case (A)

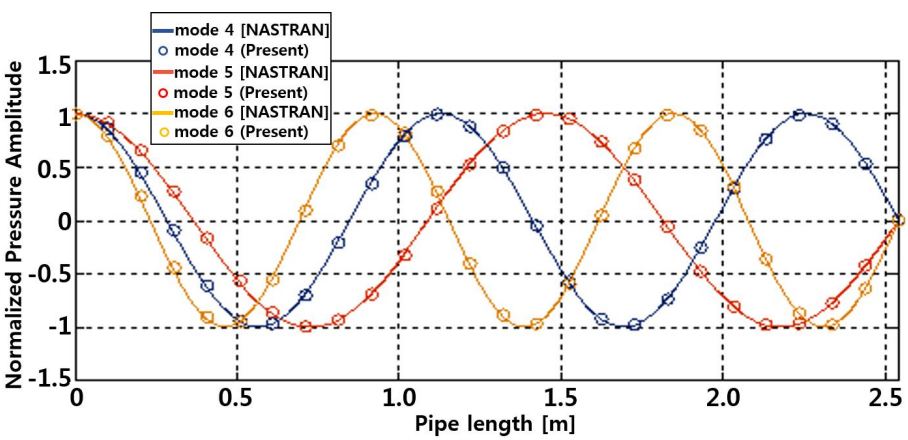

(b) Case (B)

Figure 3.4 Shapes for the 4~6th Pressure Modes

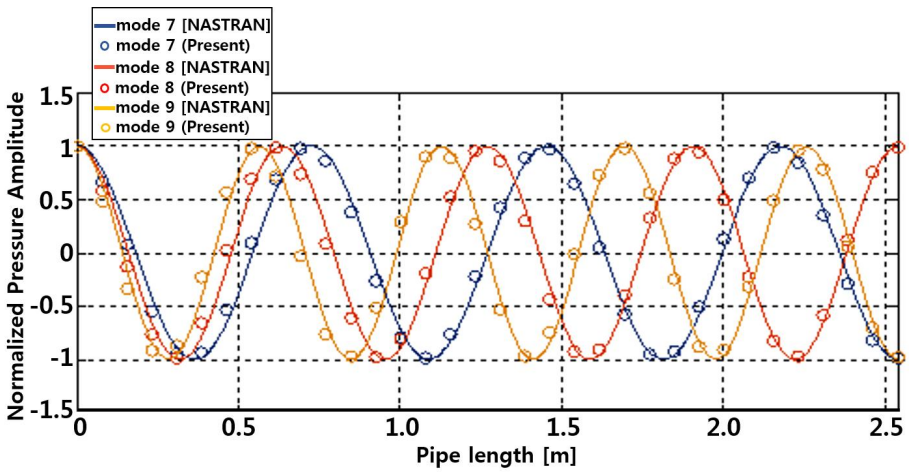

(a) Case (A)

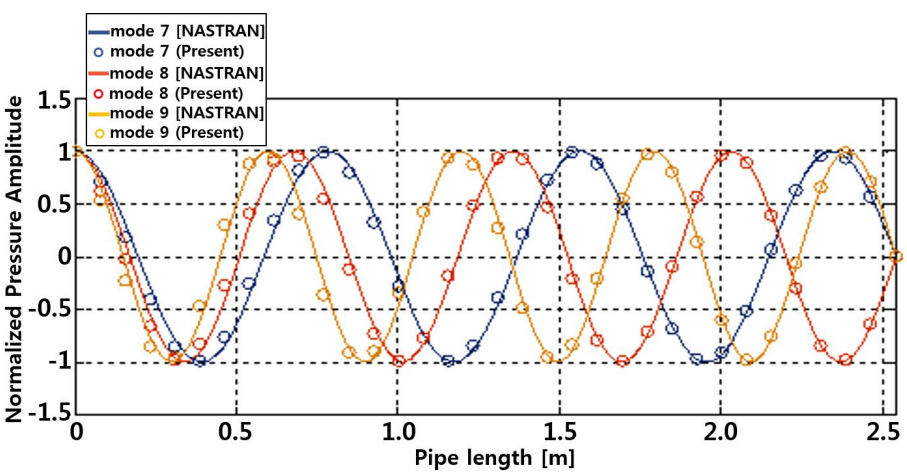

(b) Case (B)

Figure 3.5 Shapes for the 7~9th Pressure Modes

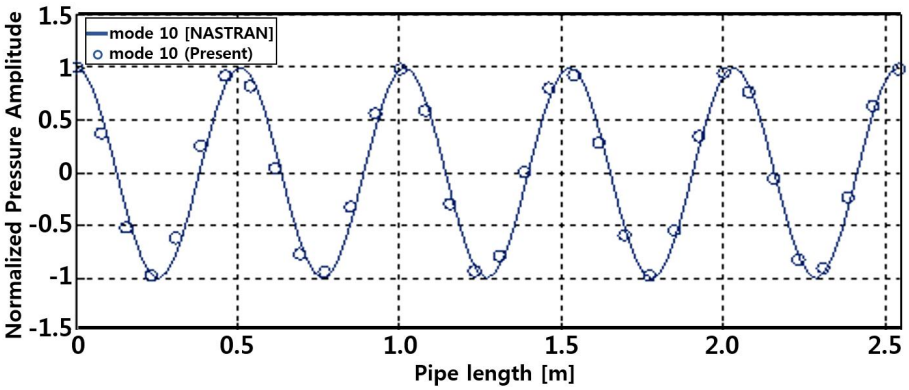

(a) Case (A)

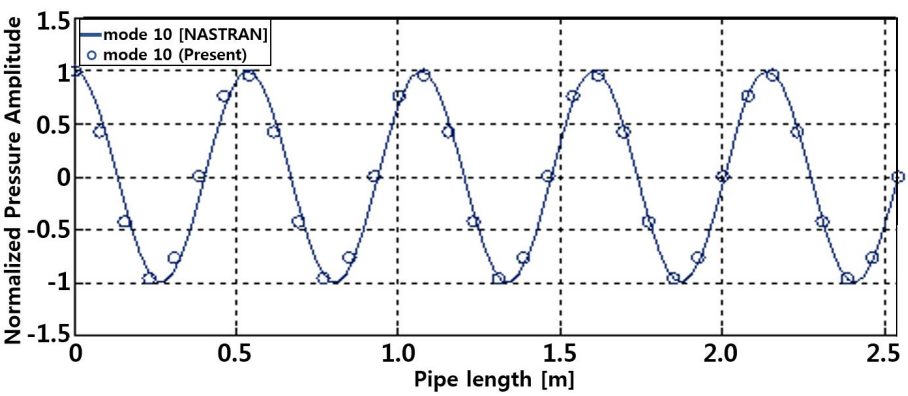

(b) Case (B)

Figure 3.6 Shapes for the 10th Pressure Modes

3.2.2 Application of the Modified Finite Element Method

In the space shuttle, the interpump line mode is a pressure mode that can be predicted because it causes resonance with the several structural modes. Therefore, it is necessary to derive the respective pressure mode considering the inertance and compliance in three flight conditions (lift off, after solid rocket booster (SRB) separation, end-burn).

In Fig. 3.7, the interpump line refers to the pipe from the inlet of the low pressure oxidizer pump (LPOP) to the inlet of the high pressure oxidizer pump (HPOP). Therefore, boundary conditions at both ends of the pipe are adjusted to the compliance of LPOP inlet and HPOP inlet. Table 3.4 shows the inertance and compliance properties of the interpump line according to the three flight times. Based on this, the present analysis can be used to predict the interpump line pressure modes numerically. Also, Eq. (34) is a formula to analytically obtain the natural frequencies of the interpump line mode, which is presented in Ref. 7. In Eq. (34), compliance C of LPOP and HPOP inlet is used as the boundary condition between the two ends of the interpump line.

$$f_{ip}(Hz) \approx \frac{1}{2\pi}\left(\frac{1/C_{b1}+1/C_{b2}}{L_{p1}+L_{ip}}\right)^{1/2} \tag{34}$$

As mentioned above, the natural frequencies of the interpump line can be obtained by the present analysis and analytical solution [7]. To find the appropriateness of the present analysis, accuracy of the prediction will be discussed

here. The natural frequency obtained by the present analysis is to be compared with the analytic solution on the interpump line presented in Eq. (34). Equation (34) is considered as a reference result. And, the analytic solution was in fact used to analyze the pogo phenomenon of the space shuttle in Ref. 7.

Table 3.5 shows that the present analysis features the reasonable discrepancies when compared with analytic solution in Ref. 7 for all flight conditions. The maximum difference is 4.1% at lift off, which is relatively small. Therefore, the present analysis is found to be useful for predicting the pressure frequencies of the interpump line.

In order to compare the mode shapes in end-burn, interpump line mode shape from Ref. 7 is illustrated in Fig. 3.8(b). And, Fig. 3.8(a) is the interpump line mode shape in end-burn predicted by the present analysis. Figure 3.8(a) shows a similar mode shape when compared with that in red box of Fig. 3.8(b). The red box in Fig. 3.8(b) is the mode shape between LPOP and HPOP inlet. Regarding the portions that are not inside the red box, the present analysis is incapable of preforming the feedline analysis. This is because there exists a nonlinear pressure perturbation inside the feedline. Therefore, mode shapes of the interpump line can be only obtained by the present analysis. In addition, the instability in which the pressure amplitude continuously increases from the LPOP inlet can be predicted by the present analysis. Thus, the reliability of the present analysis can be ascertained in the case of the space shuttle.

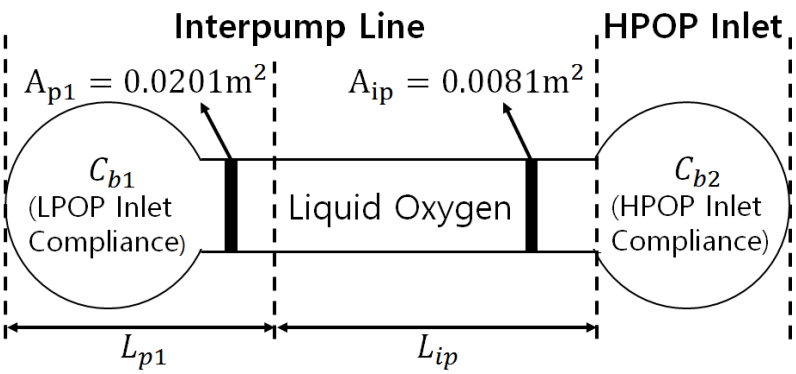

Figure 3.7 Analytic Representation of the Space Shuttle Interpump Line

Table 3.4 Inertance and Compliance Properties of Interpump Line in Three Flight Conditions

Flight Condition	Lift off	After SRB Separation	End-burn
LPOP Inlet Compliance, $C_{b1}(10^{-3}\ m^5/MN)$	1.2	2.3	0.59
HPOP Inlet Compliance, $C_{b2}(10^{-3}\ m^5/MN)$	0.27	0.3	0.24
LPOP Inertance, $L_{p1}(MNs^2/m^5)$		0.017	
Interpump Inertance, $L_{ip}(MNs^2/m^5)$		0.22	

Table 3.5 Comparison of the Present Analysis and Analytical Solution [7]

Interpump line natural frequencies [Hz]	Present analysis	Analytical solution [7]	Difference (%)
Lift off	22.9	22.0	4.1
After SRB Separation	20.9	20.1	4.0
End-burn	25.8	25.0	3.2

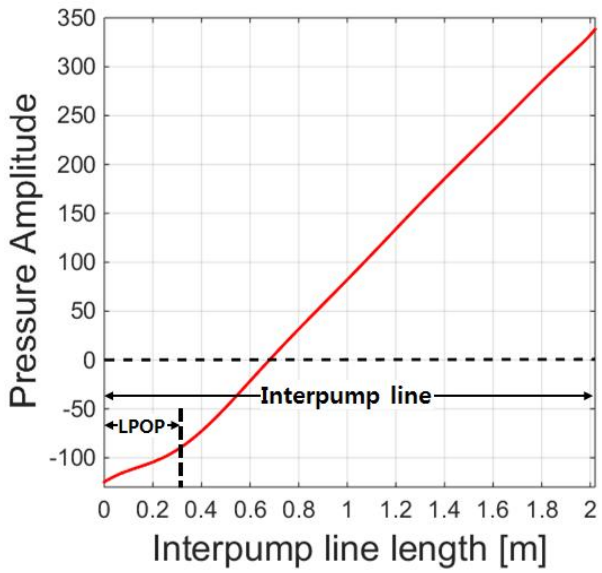

(a) Present prediction

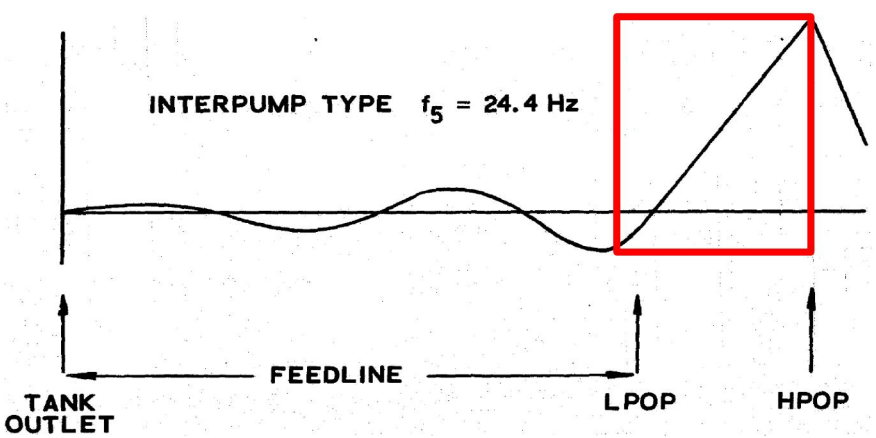

(b) Root-finding program [7]

Figure 3.8 Mode Shapes in the Interpump Line at End-burn

Chapter 4

Analysis on Pogo Suppression

4.1 Pogo Suppressor Modeling

4.1.1 Structural Gain

According to Ref. 7, a structural gain is defined when all the components of the space shuttle main engine (SSME) have one movement in the longitudinal direction.

$$G_e = \frac{\phi_e^2}{M} \tag{35}$$

In Eq. (35), ϕ_e is the modal displacement in the longitudinal direction of the engine, and M is the generalized mass of the space shuttle structural mode. Therefore, the larger the structural gain, the greater the displacement of the engine will be in the longitudinal direction. As a result, the effect on the pressure and flow rate in the engine will increase. In Ref. 7, the structural gain increased sharply when the three flight conditions (lift off, after SRB separation, and end-burn) had the structural natural frequencies greater than 20Hz. In this case, the probability of pogo occurrence increased when the feedline system pressure modes matched the structural modes with large structural gain. For this reason, if the pressure modes of the feedline system are decreased below 20Hz, it is expected that the resonance

with the structural modes having a large structural gain will be avoided, thereby avoiding the pogo.

4.1.2 Modeling of a Pogo Suppressor using a Branch Pipe

To effectively design a pogo suppressor using the modified finite element method, the concept of a branch pipe, which was suggested in Ref. 11, is used. Unlike the one-dimensional straight pipe verified in Section 3 above, a branch pipe is a method of placing a new element at a branch location so that another pipe can be connected to the middle of the pipe. A branch location is the position at which two or more pipes intersect with each other.

Figure 4.1 shows the branch location and branch pipe. In the case of a branch pipe, the boundary condition of the end can be set and analyzed by applying the inertance, compliance, and resistance properties. Thus, it is useful for analyzing additional components such as the accumulators. Hence, by applying the idea of branch pipe to the space shuttle interpump line, the accumulator can be included in the modified finite element method analysis.

In Fig. 4.2, a resistive accumulator is mounted on the HPOP inlet of the interpump line. The location and type of this accumulator are selected based on Ref. 7. The accumulator effectively suppressed the pogo instability of the space shuttle interpump line. Also, the parameters used in the analysis of the accumulator are selected based on Ref. 7, and the parameters are given by Eqs. (36), (37), and (38).

$$C_a = 0.006 m^5 / MN \tag{36}$$

$$R_a = 1.7 MNs / m^5 \tag{37}$$

$$L_a = 0.023 MNs^2 / m^5 \tag{38}$$

Unlike the other pogo suppressors, the resistive accumulator has a non-

negligible resistance property. In Fig. 4.2, LPOP and interpump line are analyzed as undamped system, and the resistive accumulator is interpreted as a damped system. In the case of the damped system, the eigenvalue analysis is performed considering the H value, i.e., the damping matrix $[D]$, in Eq. (30).

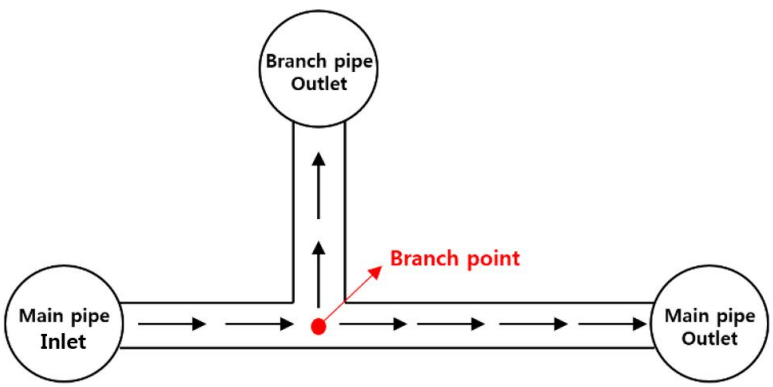

Figure 4.1 Analytic Representation of the Branch Pipe

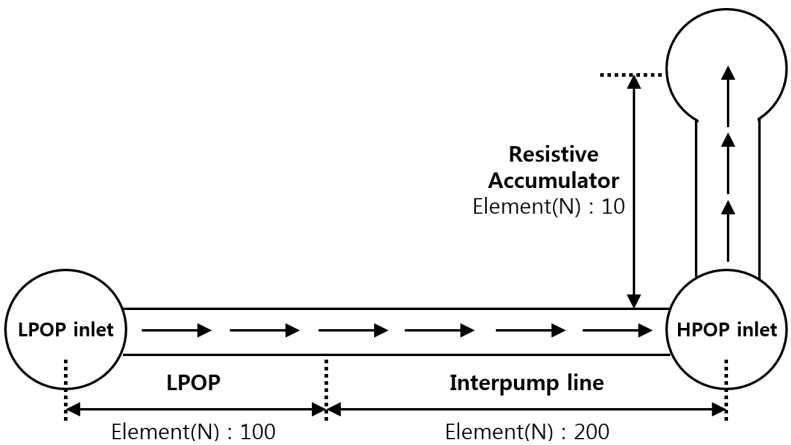

Figure 4.2 Interpump Line using a Resistive Accumulator

4.2 Demonstration of Pogo Suppression

As shown in Table 4.1, when the resistive accumulator is installed, the natural frequencies of the interpump line in each flight condition will decrease below 20Hz. Therefore, as mentioned in Section 4.1.1, the interpump line modes can avoid the resonance with the structural modes when the structural gain is relatively large.

In addition, the interpump line modes, which increases the pressure amplitudes, can also cause instability when resonating with the structural modes. Therefore, the pressure amplitude of the interpump line with a resistive accumulator is predicted. In Fig. 4.3, the mode shapes for all three flight conditions exhibit a reduced pressure amplitude. The reduction rate based on the maximum value of the pressure amplitude is as follows. The reduction percentage for lift off is 87.2%, that after SRB separation is 79.5% and that for end-burn is 92.9%. These numerical results suggest that the interpump line has a range of pressure amplitudes stable from the pogo. For this reason, the resistive accumulator is capable of suppressing the instability.

Table 4.1 Comparison of the Interpump Line Natural Frequencies including the Resistive Accumulator

Interpump line natural frequencies [Hz]	Without the resistive accumulator, Ref. 7	With the resistive accumulator, present analysis
Lift-off	**22.0**	**18.4**
After SRB Separation	**20.1**	**18.3**
End-burn	**25.0**	**18.4**

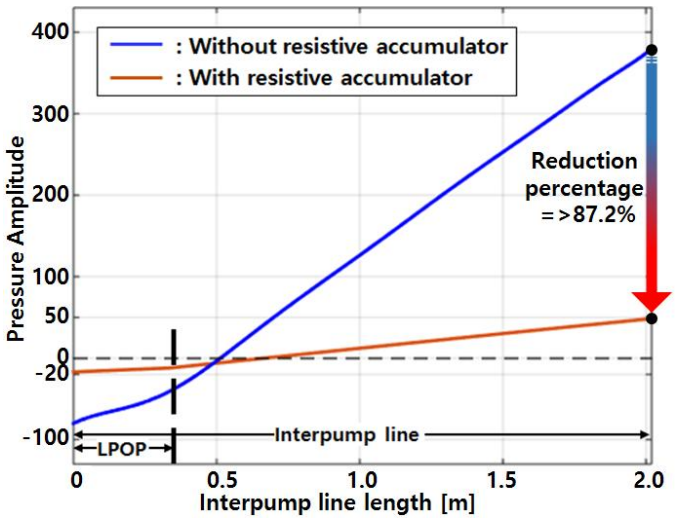

(a) Lift off

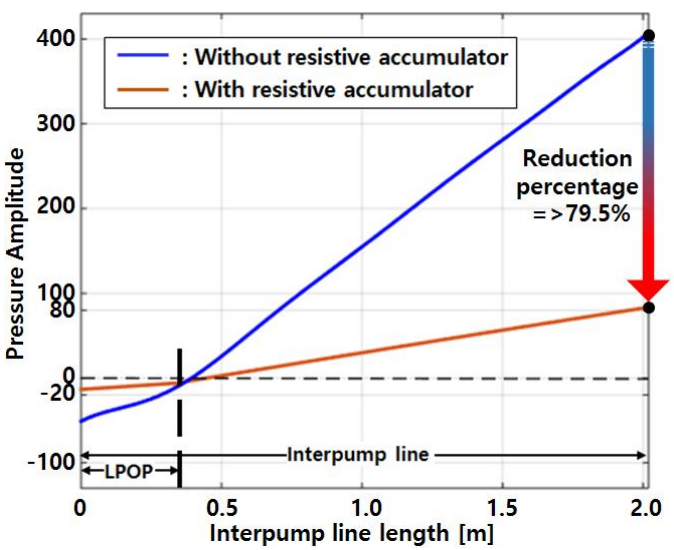

(b) After SRB Separation

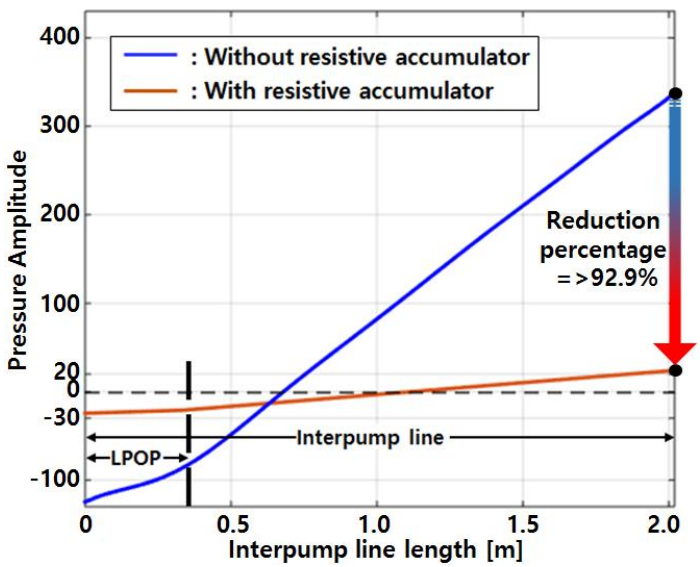

(c) End-burn

Figure 4.3 Comparison of Interpump Line Mode Shapes with and without the Resistive Accumulator

Chapter 5

Conclusion and Future Works

5.1 Conclusion

In this thesis, dynamic analyses of the tank with fluid and feedline are developed to predict the pogo phenomenon in space launch vehicle. During the development of the space shuttle, resonance was predicted in the interpump line in LOX system. Such resonance can cause the pogo phenomenon. Therefore, this thesis focuses on the numerical analysis of the longitudinal vibration mode at LOX tank and the interpump line pressure modes.

The longitudinal mode of the tank including liquid oxygen was analyzed in order for the pogo prediction in a space launch vehicle. With the assumptions of 1) an incompressible flow, 2) an inviscid flow, 3) surface pressure of the propellant in the tank is zero, 4) displacement of the fluid surface is perpendicular to the fluid surface, the propellant in the tank can be represented simply by a fluid mass matrix. The virtual mass method analyzes the fluid in the tank by a simple mass matrix, reflecting the four assumptions above. This method was then applied to validate a small hemispherical tank and to analyze a 1/8-scale space shuttle external tank including LOX tank. The verification result converged with the experimental results. The longitudinal mode of the external tank was then analyzed according to

the height of the liquid. These results were similar to previous NASA investigations, even while considering that the tank was a simplified configuration which differed from the actual shape.

Next, the analysis on the pressure mode of interpump line in space shuttle was conducted. The present analysis was constructed by using the modified finite element method, which is improved further from the conventional finite element method. This analysis defines the boundary conditions at both ends of the fluid as an expression for the length and volume of the element. The pressure modes of the helium gas were verified using present analysis. The numerical results and the NASTRAN program was found to be in good agreement. And, the pressure modes of the interpump line were predicted. The present analysis provided accurate natural frequencies when compared with the existing analytic solution. The predicted mode shapes are also similar to those of the existing result.

Furthermore, an accumulator was examined to suppress the pogo phenomenon in the interpump line. A resistive accumulator was applied to the interpump line using the idea of a branch pipe. The present analysis considering the resistive accumulator decreased the natural frequencies of the interpump line below resonance area where the structural gain of the structural mode is large. Also, it was found that the pressure amplitude of the interpump line is greatly reduced. As a result, the capability of suppressing the pogo was ascertained.

Therefore, the virtual mass method and present analysis using modified finite element method are useful for predicting the occurrence and suppression of the

pogo phenomenon. By the present procedure, it is expected that the pogo phenomenon in arbitrary launch vehicles can be analyzed.

5.2 Recommendation for Future Works

The following two items are recommended:

1) In the space shuttle, pogo instability is found in the feedline between the tank and the pump. This phenomenon occurs mainly when the primary modes of the launch vehicle structure coincided with those of the feedline. Therefore, the primary modes of the feedline will be reflected in the present analysis, and the research will be carried out to enable the modal analysis.
2) The pressure change of the feedline inlet is influenced by the pressure of the LOX tank outlet. By considering the LOX tank outlet pressure, the effect of the tank on the feedline can be evaluated accurately. The LOX tank outlet pressure will be analyzed by the virtual mass method. Thus, coupling analysis between the launch vehicle tank structure and feedline system will be possible.

References

[1]Kana, D. D., Nagy, A., “An experimental study of axisymmetric modes in various propellant tanks containing liquid,” Technical Report, SwRI Project No. 02-2583, May 1971.

[2]Rubin, S., “Longitudinal Instability of Liquid Rockets Due to Propulsion Feedback (POGO), Journal of Spacecraft and Rockets, Vol. 3, No. 8, 1966, pp. 1188-1195.

[3]Bernstein, M., Coppolino, R., Zalesak, J., and Mason, P. W., “Development of technology for fluid-structure interaction modeling of a 1/8-scale dynamic model of the shuttle external tank(ET)”, Technical Report, NASA CR-132549, August 1974.

[4]Coppolino, R., “A Numerically Efficient Finite Element Hydroelastic Analysis. Volume 1: Theory and Results”, Technical Report, NASA CR-2662, April 1976.

[5]Coppolino, R., “A Numerically Efficient Finite Element Hydroelastic Analysis. Volume 2: Implementation in NASTRAN”, Technical Report, NASA CR-2662, April 1974.

[6]Blanchard, U. J., Miserentino, R., and Leadbetter, A., “Experimental Investigation of the Vibration Characteristics of a Model of an Asymmetric Multielement Space”, Technical Report, NASA TN D-8448, September 1977.

[7]Lock, M. H., and Rubin, S., “Passive Suppression of Pogo on the Space Shuttle“, NASA CR-132452, 1974.

[8]Lock, M. H., and Rubin, S., "Analysis of Pogo on the Space Shuttle: Accumulator Design Guidelines and Planar Multiengine Model," Technical Report, NASA CR-151135, September 1976.

[9]Oppenheim, B. W., and Rubin, S., "Advanced Pogo Stability Analysis for Liquid Rockets", Journal of Spacecraft and Rockets, Vol. 30, No. 3, May-June 1993.

[10]Larsen, C. E., "NASA Experience with Pogo in Human Spaceflight Vehicles," NATO RTO Symposium ATV-152 on Limit-Cycle Oscillations and Other Amplitude-Limited, Self-Excited Vibrations, May 5-8, 2008, Norway.

[11]Michalopoulos, C. D., Clark, R. W., Doiron, H. H., "Fourth Annual Thermal and Fluids Analysis Workshop: Acoustic Modes in Fluid Networks," NASA Conference, 1992, Cleveland, Ohio, US.

[12]Lee, S. G., Sim, J. S., and Shin, S. J., "Comparison and Application of Virtual Mass Method and Phantom Boundary for Hydroelastic Analyses for Three-Dimensional Tanks", KSAS 2016 Fall Conference, Jeju, Korea, 2016.

[13]Sim, J., Kim, J., Lee, S., Shin, S., Choi, H., and Yoon, W., "Further Extended Structural Modeling and Modal Analysis of Liquid Propellant Launch Vehicles for Pogo Analysis," AIAA SPACE 2016 Conference and Exposition, Sep 12-16, 2016, Long Beach, CA.

[14]Kim, J., Sim, J., Lee, S., Shin, S., Park, J., Kim, Y., "Integrated One-dimensional Dynamic Analysis Methodology for Space Launch Vehicles Reflecting Liquid Components," The Aeronautical Journal, 2017, Online Published.

국문초록

가상질량기법과 개선된 유한요소법을 이용한 우주 발사체의 포고 현상 예측

이 상 구

기계항공공학부

서울대학교 대학원

우주 발사체에서 동체 구조 및 공급계 사이의 연성(coupling)에 의해 발생할 수 있는 여러 불안정 현상이 존재한다. 그러므로, 우주 발사체 개발과정에서 다양한 불안정 현상을 예측하는 것이 중요하다. 포고현상은 그러한 연성 불안정 현상 중 한 가지이다. 이 현상은 발사체 구조의 축방향 진동모드가 공급/추진계 공급라인의 압력 및 유량모드와 공진하고, 이러한 공진이 동체구조를 다시 가진시키는 불안정 현상이다. 포고해석을 위해서, 액체 추진제를 반영한 발사체 구조모드와 공급/추진계 내 공급라인 압력모드의 정확한 해석이 필수적이다.

본 논문에서는 액체를 포함한 3 차원 탱크의 구조 진동해석을 수행하고, 발사체 공급라인의 압력모드를 예측하였다. 그리고, 공급계에 포고억제기를 적용함으로써, 포고의 예방을 제시하였다.

액체를 포함한 탱크는 우주 발사체에서 많은 부피를 차지하기 때문에 가상질량기법을 이용하여 3 차원 탱크의 구조 진동해석을 수행하였다. 이

기법의 정확성을 입증하기 위해, 우주왕복선 외부탱크의 1/8-scale 소규모 형상이 사용되었다. 특히, 외부탱크 안에 있는 액화산소 탱크를 본격적으로 해석하였다. 고유진동수와 모드형상이 이전 연구자들의 예측 결과와 잘 일치함을 확인하였다.

공급계에서는, 개선된 유한요소법을 이용한 present analysis 가 우주왕복선의 불안정 현상을 유발하는 interpump line 의 압력모드를 예측하는 업무에 적용되었다. 개선된 유한요소법은 NASTRAN 해석을 통하여 입증되었고, 우주왕복선 LOX 시스템의 interpump line 에 적용되었다. 수치적 결과와 우주왕복선에 관한 참고문헌의 비교 결과 적절할 수준이었다.

마지막으로, 포고 억제기가 우주왕복선의 interpump line 에 적용되었다. 그 결과, interpump line 의 고유진동수를 변경시킴으로써 동체 구조와의 공진가능성이 감소하였다. 그러므로, 포고 억제능력이 시현되었다.

주요어 : 우주 발사체, 포고 현상, 축방향 동적 해석, 가상질량기법, 공급라인 압력 모드, 개선된 유한요소법, 포고 억제기

학 번 : 2016-20747